INTERNATIONAL JOURNAL FOR NUMERICAL METHODS IN FLUIDS, VOL. 7, 603–619 (1987)

TWO-DIMENSIONAL NUMERICAL CALCULATION OF THE FLOW FIELD ABOUT A SCOOP INLET BY THE PIECEWISE LINEAR METHOD

HISASHI MIKAMI

Research Laboratory for Nuclear Reactors, Tokyo Institute of Technology, Ookayama, Meguro-ku, Tokyo, Japan

SUMMARY

The piecewise linear method (PLM) based on time operator splitting is used to solve the unsteady compressible Euler equations describing the two-dimensional flow around and through a straight wall inlet placed stationary in a rapidly rotating supersonic flow. The PLM scheme is formulated as a Lagrangian step followed by an Eulerian remap. The inhomogeneous terms in the Euler equations written in cylindrical co-ordinates are first removed by Sod's method and the resulting set of equations is further reduced to two sets of one-dimensional Lagrangian equations, using time operator splitting. The numerically generated flow fields are presented for different values of the back pressure imposed at the downstream exit of the inlet nozzle. An oblique shock wave is formed in front of the almost whole portion of the inlet entrance, the incoming streamlines being deflected towards the higher pressure side after passing through the oblique shock wave and then bending down to the lower pressure side. A reverse flow appears inside the inlet nozzle owing to the recovery pressure of the incoming streams being lower than the back pressure of the inlet nozzle.

KEY WORDS PLM Scheme, Rotating Flow, Supersonic Flow, Numerical Calculation, Shock Wave, Unsteady Compressible Euler Equations

INTRODUCTION

In achieving the desired performance of a gas centrifuge for uranium enrichment, proper design of the stationary Pitot-like tubes (so-called scoops) inside the rotating cylinder is one of the most important factors. The scoops extract the heavy and the light gases separated by the centrifugal force and induce a recirculating flow by reducing the angular velocity of the rotating gas about the scoops. The recirculating flow is essential to accomplish considerable separation in a single machine. The gas flow through the scoops with maximum total pressure recovery and the drag moment adequate to create the optimum recirculating mass flow are required for design conditions of the centrifuge. To meet these requirements, detailed calculations of the flow field around and through the scoop inlet are necessary. The inlet flow field is, of course, three-dimensional and complex, owing to the formation of shock waves. The complexities are further increased by the fact that the flow field is influenced by the stratification in the free stream.

In a previous paper,[1] a numerical analysis of the flow near a scoop inlet was presented by numerically solving the Euler equations using the Beam–Warming scheme. A simplification was made by considering the flow in the symmetry planes, where the flow can be regarded as two-dimensional (Figure 1). A further simplification was that of negligible velocity gradient normal to the planes, and the flow was assumed to be described by the Euler equations for planar flow

0271–2091/87/060603–17$08.50

Received 1 July 1986
Revised 10 October 1986

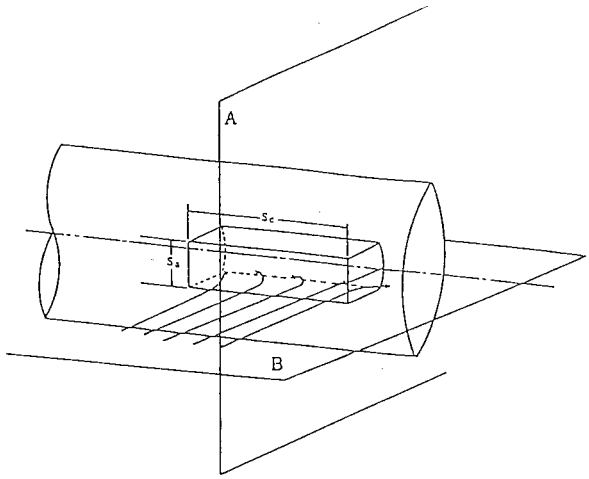

Figure 1. Planes of symmetry of the flow field about the scoop inlet

although we could take the normal velocity gradient into account by using the velocity distributions in the planes themselves. The steady solutions were presented for various values of the back pressure imposed at the downstream of the scoop inlet. It was found that the stratification of the incoming stream has significant effects on the flow field; that is the shock wave shapes and the velocity distributions around the inlet nozzle differ from those formed in the uniform supersonic stream.

In the present work, the inlet flow fields in a rotating supersonic stream are calculated by the piecewise linear method developed by Van Leer.[2] Although geometrical and physical simplifications are similar to those made in the previous paper,[1] there are substantial differences in the present calculations. These are

1. Bluntness of the scoop leading edge is taken into account.
2. The top boundary is located four inlet-spans away from the scoop in the direction transverse to the incoming stream. Thus, shock waves do not cross the top boundary, where the flow variables are determined assuming a solid-body rotation.
3. The bottom boundary is the wall of the rotating cylinder, where the reflecting boundary conditions are imposed.
4. The piecewise linear method (PLM) based on time operator splitting is used to solve the unsteady equations of motion describing the transonic flow of inviscid and non-heat-conducting gas.
5. The results of calculation are presented by contour plots of the pressure fields as well as the velocity vector representation.

GOVERNING EQUATIONS

Since the main building block is the Lagrangian equations of motion for an inviscid, non-heat-conducting, compressible gas, we shall first derive these equations from the Eulerian equations normally used for the numerical computation of non-stationary flow fields.

The continuity, momentum and energy equations in cylindrical co-ordinates can be written in the conservative form:

$$\frac{\partial \rho}{\partial t} + \frac{\partial \rho u}{\partial r} + \frac{1}{R}\frac{\partial \rho v}{\partial \theta} = -\frac{\rho u}{R}, \tag{1}$$

$$\frac{\partial \rho u}{\partial t} + \frac{\partial (\rho u^2 + \kappa p)}{\partial r} + \frac{\partial \rho uv}{R\partial \theta} = -\frac{\rho}{R}(u^2 - v^2), \tag{2}$$

$$\frac{\partial \rho v}{\partial t} + \frac{\partial \rho uv}{\partial r} + \frac{\partial (\rho v^2 + \kappa p)}{R\partial \theta} = -\frac{2\rho uv}{R}, \tag{3}$$

$$\frac{\partial \rho E}{\partial t} + \frac{\partial u(\rho E + \kappa p)}{\partial r} + \frac{\partial v(\rho E + \kappa p)}{R\partial \theta} = -\frac{u(\rho E + \kappa p)}{R}, \tag{4}$$

with

$$E = \frac{p}{2\gamma\rho} + \tfrac{1}{2}(u^2 + v^2), \tag{5}$$

where ρ, u, v, p and E denote the density, the radial velocity, the azimuthal velocity, the pressure and the total energy per unit mass, respectively, made dimensionless by the corresponding dimensional quantities denoted by bars:

$$\bar{u} = \bar{q}_{\max,e} u, \quad \bar{v} = \bar{q}_{\max,e} v,$$
$$\bar{p} = \bar{p}_{0,e} p, \quad \bar{\rho} = \bar{\rho}_{0,e} \rho,$$
$$\bar{E} = E\bar{\rho}_{0,e}\bar{q}^2_{\max,e}, \quad \bar{r} = \bar{W} r,$$
$$\bar{s} = \bar{W} s,$$

where $q_{\max}$ is the limit speed, p_0 is the stagnation pressure, ρ_0 is the stagnation density, $\bar{W}$ is the width of the inlet nozzle, and the subscript 'e' denotes the peripheral flow quantities of the free stream, rotating at the given rotational Mach number; κ is defined by $\kappa = (\gamma - 1)/2\gamma$, where γ is the ratio of specific heats. The azimuthal metric coefficient, r, is assumed equal to the radius of the rotating cylinder, R, since the scoop inlet is located near the periphery. This approximation introduces a significant simplification into the numerical algorithm. The geometry and the cylindrical co-ordinate system are shown in Figure 2.

Inhomogeneous terms in equations (1)–(4) can be removed by applying time operator splitting (the method of Sod[3]). The resulting set of equations takes the form

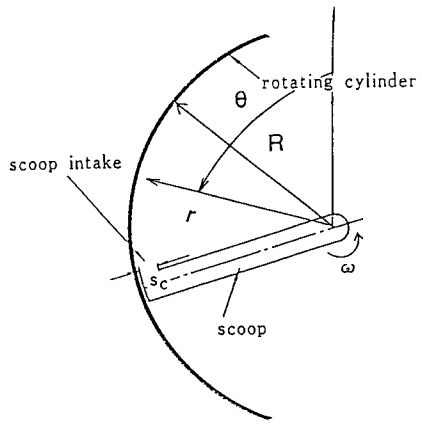

Figure 2. Geometry and the cylindrical co-ordinate system

$$\frac{\partial \rho}{\partial t} + \frac{\partial \rho u}{\partial r} + \frac{\partial \rho v}{\partial s} = 0, \tag{6}$$

$$\frac{\partial \rho u}{\partial t} + \frac{\partial (\rho u^2 + \kappa p)}{\partial r} + \frac{\partial \rho uv}{\partial s} = 0, \tag{7}$$

$$\frac{\partial \rho v}{\partial t} + \frac{\partial \rho uv}{\partial r} + \frac{\partial (\rho v^2 + \kappa p)}{\partial s} = 0, \tag{8}$$

$$\frac{\partial \rho E}{\partial t} + \frac{\partial u(\rho E + \kappa p)}{\partial r} + \frac{\partial v(\rho E + \kappa p)}{\partial s} = 0, \tag{9}$$

$$\frac{\mathrm{d}\rho}{\mathrm{d}t} = -\frac{\rho u}{R}, \tag{10}$$

$$\frac{\mathrm{d}\rho u}{\mathrm{d}t} = -\frac{\rho(u^2 - v^2)}{R}, \tag{11}$$

$$\frac{\mathrm{d}\rho v}{\mathrm{d}t} = -\frac{2\rho uv}{R}, \tag{12}$$

$$\frac{\mathrm{d}\rho E}{\mathrm{d}t} = -\frac{u(\rho E + \kappa p)}{R}, \tag{13}$$

with

$$s = R\theta. \tag{14}$$

The second step is to use operator splitting to reduce equations (6)–(9) to the separate equations in one-dimensional form:

$$\frac{\partial \rho}{\partial t} + \frac{\partial \rho u}{\partial r} = 0, \tag{15}$$

$$\frac{\partial \rho u}{\partial t} + \frac{\partial (\rho u^2 + \kappa p)}{\partial r} = 0, \tag{16}$$

$$\frac{\partial \rho v}{\partial t} + \frac{\partial \rho uv}{\partial r} = 0, \tag{17}$$

$$\frac{\partial \rho E}{\partial t} + \frac{\partial u(\rho E + \kappa p)}{\partial r} = 0, \tag{18}$$

$$\frac{\partial \rho}{\partial t} + \frac{\partial \rho v}{\partial s} = 0, \tag{19}$$

$$\frac{\partial \rho u}{\partial t} + \frac{\partial \rho uv}{\partial s} = 0, \tag{20}$$

$$\frac{\partial \rho E}{\partial t} + \frac{\partial v(\rho E + \kappa p)}{\partial s} = 0. \tag{21}$$

These equations are further rewritten in the following non-conservative form:

$$\frac{\partial \rho}{\partial t} + u\frac{\partial \rho}{\partial r} + \rho\frac{\partial u}{\partial r} = 0, \tag{22}$$

$$\rho\left(\frac{\partial u}{\partial t}+u\frac{\partial u}{\partial r}\right)+\frac{\partial \kappa p}{\partial r}=0, \tag{23}$$

$$\rho\left(\frac{\partial v}{\partial t}+u\frac{\partial v}{\partial r}\right)=0, \tag{24}$$

$$\rho\left(\frac{\partial E}{\partial t}+u\frac{\partial E}{\partial r}\right)+\frac{\partial \kappa u p}{\partial r}=0, \tag{25}$$

$$\frac{\partial \rho}{\partial t}+v\frac{\partial \rho}{\partial s}+\rho\frac{\partial v}{\partial s}=0, \tag{26}$$

$$\rho\left(\frac{\partial u}{\partial t}+v\frac{\partial u}{\partial s}\right)=0, \tag{27}$$

$$\rho\left(\frac{\partial v}{\partial t}+v\frac{\partial v}{\partial s}\right)+\frac{\partial \kappa p}{\partial s}=0, \tag{28}$$

$$\rho\left(\frac{\partial E}{\partial t}+v\frac{\partial E}{\partial s}\right)+\frac{\partial \kappa v p}{\partial s}=0. \tag{29}$$

We now introduce the mass co-ordinates,

$$\xi=\int_{r_0}^{r}\rho\,\mathrm{d}r \tag{30}$$

and

$$\eta=\int_{s_0}^{s}\rho\,\mathrm{d}s. \tag{31}$$

Then, the independent variables are changed to ξ, η, t, and the density ρ is replaced by the specific volume τ. In terms of these variables, equations (22)–(29) reduce to

$$\frac{\partial \tau}{\partial t}-\frac{\partial u}{\partial \xi}=0, \tag{32}$$

$$\frac{\partial u}{\partial t}+\frac{\partial \kappa p}{\partial \xi}=0, \tag{33}$$

$$\frac{\partial v}{\partial t}=0, \tag{34}$$

$$\frac{\partial E}{\partial t}+\frac{\partial \kappa u p}{\partial \xi}=0, \tag{35}$$

$$\frac{\partial \tau}{\partial t}-\frac{\partial v}{\partial \eta}=0, \tag{36}$$

$$\frac{\partial u}{\partial t}=0, \tag{37}$$

$$\frac{\partial v}{\partial t}+\frac{\partial \kappa p}{\partial \eta}=0, \tag{38}$$

$$\frac{\partial E}{\partial t}+\frac{\partial \kappa v p}{\partial \eta}=0. \tag{39}$$

The above equations together with equations (10)–(13) are the basic equations used in the present numerical computations.

INITIAL AND BOUNDARY CONDITIONS

At the start of calculation, a complete initial flow field must be provided at all computational meshes. The initial flow field in the free stream is calculated, assuming a solid-body rotation:

$$p=\frac{1}{\left(1+\dfrac{\gamma-1}{2}M_{\mathrm{R}}^2\right)^{\gamma/(\gamma-1)}}\mathrm{e}^{1/2[\gamma M_{\mathrm{R}}^2(\sigma^2 r^2-1)]}, \tag{40}$$

$$T=\frac{1}{\left(1+\dfrac{\gamma-1}{2}M_{\mathrm{R}}^2\right)}, \tag{41}$$

$$u=0, \tag{42}$$

$$v=\left(\frac{\gamma-1}{2}\right)^{1/2}\frac{M}{\left(1+\dfrac{\gamma-1}{2}M^2\right)^{1/2}}, \tag{43}$$

$$M=M_{\mathrm{R}}\sigma r, \tag{44}$$

where σ is the ratio of the inlet width to the radius of the rotating cylinder, and the rotational Mach number, M_{R}, is defined in terms of the peripheral velocity of the rotating cylinder. Immediately downstream of the shock wave, flow variables are determined using a prescribed shock shape and the Rankine–Hugoniot shock relations. The shock wave shape is assumed to be described in terms of Cartesian co-ordinates, x, y by

$$y=-\frac{b}{x_1^2}x^2+b, \tag{45}$$

as shown in Figure 3, where the stand-off distance, b, and the half width, x_1, at the entrance

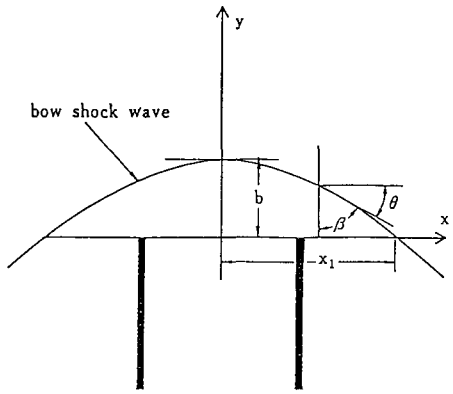

Figure 3. Shock wave generated by a parabola

plane of the inlet are guessed from the shock wave shape ahead of a flat-faced blunt body in a uniform supersonic stream. From equation (45), the shock angle β is determined by

$$\beta = \frac{\pi}{2} - \tan^{-1}\left(\frac{2b}{x_1^2}x\right). \tag{46}$$

Downstream of the shock wave, the values of the flow field are calculated by linearly interpolating the values at the shock wave and at the outflow boundary where free stream values are initially specified. At the outlet of the scoop nozzle, the static pressure, p_B is prescribed and other flow variables are obtained from the steady-state forms of the governing equations, assuming uniform parallel outflow.

The boundary conditions on the solid boundaries are determined from the reflection principle, and the flow properties at the downstream boundary external to the inlet nozzle are calculated by the zeroth-order extrapolation from the interior. The boundary conditions on the upstream and upper boundaries are evaluated assuming a solid-body rotation.

SOLUTION PROCEDURE AND THE NUMERICAL SCHEME

To solve the system of basic equations, the one-dimensional problem in the ξ-direction is solved using equations (32)–(35) in a first step, and the provisional values are corrected in a second step using equations (36)–(39) in the η-direction. The final values are calculated by solving the system of ordinary differential equations, (10)–(13), using the above solutions to determine the inhomogeneous terms.

The method used to solve the one-dimensional problem is a modified version of the PLM (piecewise linear method) algorithm formulated as a Lagrangian step, followed by an Eulerian remap.[2] The method is outlined as follows. The Eulerian space grid is equally spaced, as shown in Figure 4, where zones are denoted by suffixes j and boundaries are distinguished by $\frac{1}{2}$ integers, $j+\frac{1}{2}$. To calculate the zone average values of the specific volume τ_j^{n+1}, the velocity, u_j^{n+1} and the total energy, E_j^{n+1} at $t^{n+1} = t^n + \Delta t$, from the known values at the time $t = t^n$, the equations (32), (33), (35) are approximated by the following difference equations:

$$\tau_j^{n+1} = \tau_j^n + \frac{\Delta t}{\Delta_j \xi}(\bar{u}_{j+1/2} - \bar{u}_{j-1/2}), \tag{47}$$

$$u_j^{n+1} = u_j^n - \frac{\Delta t}{\Delta_j \xi}\kappa(\bar{p}_{j+1/2} - \bar{p}_{j-1/2}), \tag{48}$$

$$E_j^{n+1} = E_j^n - \frac{\Delta t}{\Delta_j \xi}\kappa(\bar{u}_{j+1/2}\bar{p}_{j+1/2} - \bar{u}_{j-1/2}\bar{p}_{j-1/2}), \tag{49}$$

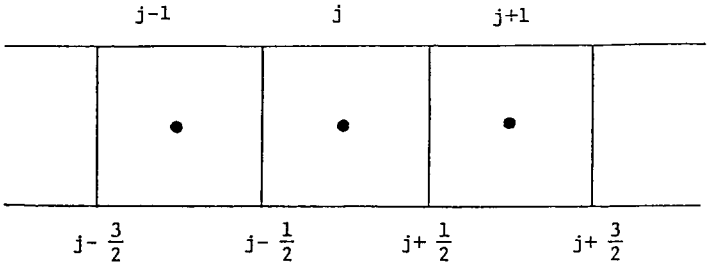

Figure 4. Eulerian space grids

where $\bar{u}_{j+1/2}$ and $\bar{p}_{j+1/2}$ are the time-averaged values for the velocity and pressure at the edges of zones. Since the Euler co-ordinate of an interface, $r_{j+1/2}$ is updated according to

$$r_{j+1/2}^{n+1} = r_{j+1/2}^{n} + \bar{u}_{j+1/2}\Delta t, \tag{50}$$

equation (47) can be rewritten in the form

$$\tau_j^{n+1} = \frac{1}{\Delta_j \xi}(r_{j+1/2}^{n+1} - r_{j-1/2}^{n+1}). \tag{51}$$

The velocity component in the η-direction, v, remains unchanged during the time step, as seen from equation (34).

The values of $\bar{u}_{j+1/2}$ and $\bar{p}_{j+1/2}$ are obtained following the procedure described by Colella and Woodward,[4] by first calculating averages of the dependent variables over the spatial domains which can influence the zone edge during the time step, whereas in the present computation piecewise linear profiles of flow variables are assumed in each zone (see Figure 5). The interaction of the two averaged states, $S_L(\rho_L, u_L, p_L)$ and $S_R(\rho_R, u_R, p_R)$ adjacent to the interface is described by a solution to Riemann's problem. The method of solving a Riemann problem is briefly described below. In the Lagrangian formulation, the zone interface is always a contact discontinuity with $u = \bar{u}$ and $p = \bar{p}$ after breakdown of the interface. The left and right states, S_L and S_R are separated from an intermediate state, $\bar{S}$, by waves, W_L and W_R which may be either shock waves or rarefaction waves, depending on the relative values of the left and right states. Across waves, the following jump conditions can be derived from the integral form of the conservation laws:

$$W_L(u_L - \bar{u}) - \kappa(\bar{p} - p_L) = 0, \tag{52}$$

$$W_R(\bar{u} - u_R) - \kappa(\bar{p} - p_R) = 0, \tag{53}$$

where W_L and W_R are the speeds of waves propagating into the left and right directions, respectively. According as $\bar{p} \geqslant p_k$ or $\bar{p} < p_k (k = L, R)$,

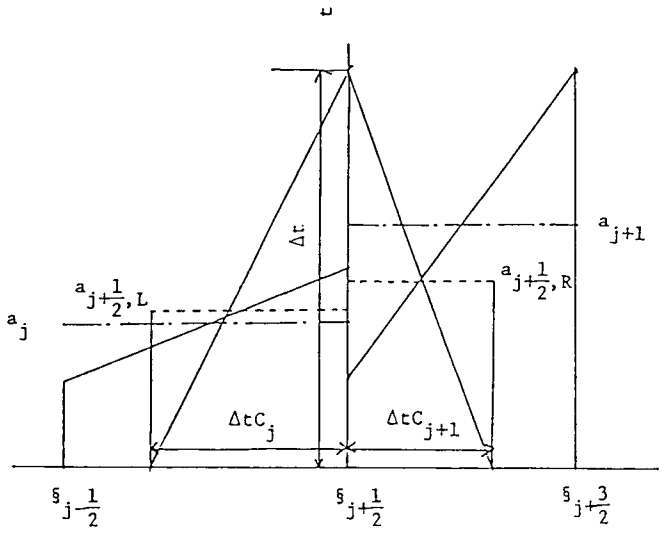

Figure 5. Average of dependent variables over the domain of dependence

$$W_k = \left(\frac{\gamma-1}{2\gamma}\right)^{1/2}\left(\frac{\gamma p_k}{\tau_k}\right)^{1/2}\left[1+\frac{\gamma+1}{2\gamma}\left(\frac{\bar{p}-p_k}{p_k}\right)\right]^{1/2}, \tag{54}$$

or

$$W_k = \left(\frac{\gamma-1}{2\gamma}\right)^{1/2}\left(\frac{\gamma p_k}{\tau_k}\right)^{1/2}\left(\frac{\gamma-1}{2\gamma}\right)\frac{\left(1-\dfrac{p}{p_k}\right)}{\left[1-\left(\dfrac{\bar{p}}{p_k}\right)^{(\gamma-1)/2\gamma}\right]}. \tag{55}$$

Solving $\bar{u}$ and $\bar{p}$ from equations (52) and (53), we obtain

$$\bar{p} = \frac{W_L W_R(u_L - u_R) + \kappa p_R W_L + \kappa p_L W_R}{\kappa(W_L + W_R)}, \tag{56}$$

$$\bar{u} = \frac{W_L u_L + W_R u_R - \kappa(p_R - p_L)}{W_L + W_R}. \tag{57}$$

Equations (54), (55) and (56) are three equations with three unknowns $\bar{p}$, W_L, W_R. These equations are solved through the iterative procedure suggested by Chorin, as described by Saito and Glass.[5] After satisfactory convergence, $\bar{u}$ is determined from equation (57).

When calculating smooth flow, the wave velocities, W_k, become nearly equal to Lagrangian sound speed C_k. Then equations (56) and (57) reduce to the difference approximation to the average form of the characteristic equations obtained from equations (32) and (33), that is

$$\mathrm{d}(u + \kappa C^{-1} p) = 0. \tag{58}$$

Given the updated zone average quantities ρ_j^{n+1}, u_j^{n+1} and p_j^{n+1}, the slopes $\Delta\rho_j^{n+1}$, Δu_j^{n+1} and Δp_j^{n+1} are calculated by centrally differencing the average values in the adjacent zones:

$$\Delta a_j^{n+1} = \frac{\Delta r_j^{n+1}}{(\Delta r_{j-1}^{n+1} + 2\Delta r_j^{n+1} + \Delta r_{j+1}^{n+1})}\left[\frac{2(\Delta r_j^{n+1} + \Delta r_{j-1}^{n+1})}{(\Delta r_{j+1}^{n+1} + \Delta r_j^{n+1})}(a_{j+1}^{n+1} - a_j^{n+1}) + \frac{2(\Delta r_j^{n+1} + \Delta r_{j-1}^{n+1})}{(\Delta r_j^{n+1} + \Delta r_{j-1}^{n+1})}(a_j^{n+1} - a_{j-1}^{n+1})\right], \tag{59}$$

where a_j^{n+1} represents ρ_j^{n+1}, u_j^{n+1}, or p_j^{n+1}. The slope of specific volume, $\Delta\tau_j^{n+1}$ is calculated by the relation

$$\Delta\tau_j^{n+1} = -\Delta\rho_j^{n+1}/(\tau_j^{n+1})^2. \tag{60}$$

On the other hand, the values of $\rho_{j+1/2}^{n+1}$, $u_{j+1/2}^{n+1}$, $v_{j+1/2}^{n+1}$ and $p_{j+1/2}^{n+1}$ at zone edges are calculated using average values and their slopes. The total energies at the zone edges, $E_{j+1/2}^{n+1}$ are then calculated by the relation

$$E_{j+1/2}^{n+1} = \frac{p_{j+1/2}^{n+1}}{2\gamma\rho_{j+1/2}^{n+1}} + \tfrac{1}{2}[(u_{j+1/2}^{n+1})^2 + (v_{j+1/2}^{n+1})^2]. \tag{61}$$

These values are then used to calculate ΔE_j^{n+1}. To suppress numerical oscillations, the monotonicity algorithms are applied to the slopes calculated above. The algebraic form of the algorithms[2] is

$$\Delta a_j^{n+1} = \min(|\Delta a_j^{n+1}|, 2|a_{j+1}^{n+1} - a_j^{n+1}|, 2|a_j^{n+1} - a_{j-1}^{n+1}|)\operatorname{sgn}(\Delta a_j^{n+1}),$$
$$\text{if} \quad \operatorname{sgn}(a_{j+1}^{n+1} - a_j^{n+1}) = \operatorname{sgn}(a_j^{n+1} - a_{j-1}^{n+1}) = \operatorname{sgn}(\Delta a_j^{n+1}), \Delta a_j^{n+1} = 0, \quad \text{otherwise.} \tag{62}$$

Table I. Computational procedures

	Given variables	Variables to be computed
Lagrangian step in the r-direction	$p, \tau, u, \Delta_r p, \Delta_r \tau, \Delta_r u$	τ, ρ, u, E, p
Eulerian remapping	$\rho, \Delta_r \rho, u, \Delta_r u, E, \Delta_r E,$ $v, \Delta_r v, \Delta_s u, \Delta_s v, \Delta_s \rho,$ $\Delta_s E$	$\rho, u, E, \tau, v, p,$ $\Delta_r \rho, \Delta_r u, \Delta_r v, \Delta_r E, \Delta_r \tau, \Delta_r p$ $\Delta_s \rho, \Delta_s u, \Delta_s v, \Delta_s E, \Delta_s \tau, \Delta_s p$
Lagrangian step in the s-direction	$p, \tau, v, \Delta_s p, \Delta_s \tau, \Delta_s v$	τ, ρ, v, E, p
Eulerian remapping	$\rho, \Delta_s \rho, v, \Delta_s v, E, \Delta_s E,$ $u, \Delta_s u, \Delta_r u, \Delta_r v, \Delta_r \rho, \Delta_r E$	$\rho, v, E, \tau, u, p,$ $\Delta_s \rho, \Delta_s u, \Delta_s v, \Delta_s E, \Delta_s \tau, \Delta_s p$ $\Delta_r \rho, \Delta_r u, \Delta_r v, \Delta_r E, \Delta_r \tau, \Delta_r p$

This limiting of the slopes guarantees that the linear distribution will not take values beyond the avearge values in the adjacent zones.

At the end of the Lagrangian step, an Eulerian zone may contain matter from adjacent zones. The new values of the conserved quantities, ρ, ρu and ρE, are computed with the aid of piecewise linear distribution by the following formulae:

$$\rho_j^{n+1} = \frac{1}{r_{j+1/2}^n - r_{j-1/2}^n} \int_{r_{j-1/2}^n}^{r_{j+1/2}^n} \rho \, \mathrm{d}r, \tag{63}$$

$$\rho_j^{n+1} u_j^{n+1} = \rho_j^{n+1} \frac{1}{\xi_{j+1/2}^{n+1} - \xi_{j-1/2}^{n+1}} \int_{\xi_{j-1/2}^{n+1}}^{\xi_{j+1/2}^{n+1}} u \, \mathrm{d}\xi, \tag{64}$$

$$\rho_j^{n+1} E_j^{n+1} = \rho_j^{n+1} \frac{1}{\xi_{j+1/2}^{n+1} - \xi_{j-1/2}^{n+1}} \int_{\xi_{j-1/2}^{n+1}}^{\xi_{j+1/2}^{n+1}} E \, \mathrm{d}\xi, \tag{65}$$

where the new mass co-ordinate, $\xi_{j+1/2}^{n+1}$, is calculated from the relation:

$$\xi_{j+1/2}^{n+1} = \xi_{j+1/2}^n - (r_{j+1/2}^{n+1} - r_{j+1/2}^n)\{\rho^{n+1} + \tfrac{1}{2}\Delta\rho_j^{n+1}[1 - (r_{j+1/2}^{n+1} - r_{j-1/2}^n)/(r_{j+1/2}^{n+1} - r_{j-1/2}^{n+1})]\}. \tag{66}$$

The above computational procedures are summarized in Table I.

These PLM schemes are implemented as a two-step method in the form

$$a^{n+1} = L_r^{\Delta t/2} L_s^{\Delta t} L_r^{\Delta t/2} a^n, \tag{67}$$

where L represents the PLM operator, the subscripts refer to the spacial direction and the superscripts denote the time increment that the solution is advanced. It is in this form that the splitting can be used to obtain an approximate solution valid to second order. Once the solution is obtained during each cycle of equation (67), the system of ordinary differential equation is solved by the Runge–Kutta–Gill method.

RESULTS AND DISCUSSION

Calculations were performed for the straight-wall inlet shown in Figure 6. The ratio of the width to the radius of the rotating cylinder is set to 0·1. The rotational Mach number is 3·0 and the

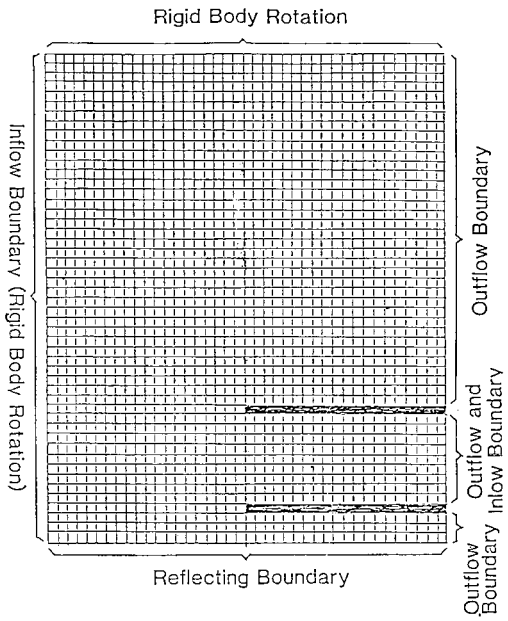

Figure 6. Computational grid and geometry of the inlet

ratio of specific heats is assumed to be 1·06. At this rotational Mach number, the inlet width normalized to the density scale height of the incoming rotating flow takes the value of 0·954.

A 51×41 grid point mesh system was used with uniform mesh increments in the r and s directions ($\Delta r = \Delta s = 0{\cdot}1$). The time step size is determined from the relation:

$$\Delta t = \mathrm{Min}\left(v\frac{\Delta r}{C}, v\frac{\Delta r}{u}, v\frac{\Delta s}{v} \right), \tag{68}$$

where the Courant number, v, is set equal to 0·5.

To study the influence of the artificial upper-wall distances on the flow solution near the scoop inlet, a series of computations was carried out by removing upper grid lines, starting from large grid system. A simple boundary condition was used at the upper boundary, setting

$$f_{1,k} = f_{2,k-1}, \tag{69}$$

when a shock wave is found to cross the boundary. This boundary condition is given by the simple wave method[6] assuming the Mach lines along the mesh diagonals. Comparisons between calculations performed with the three different mesh systems, i.e. the 61×41 grid, the 51×41 grid and the 41×41 grid in the r and s directions are presented in Figures 7–9 in terms of pressure contours. Essentially identical results are obtained even though a shock wave crosses the upper boundary for the 41×41 grid system. Thus, the 51×41 mesh system was used throughout the computation by assuming that the flow properties at the upper boundary can be evaluated on the basis of a solid-body rotation.

Figures 8, 10 and 11 show pressure contours for different values of the back pressure imposed at the outlet of the scoop nozzle. Corresponding flow patterns are shown in Figures 12–14 in terms of velocity vectors. These Figures show that both the detached bow shock wave ahead of the inlet and the expansion wave on the external wall of the inlet are well captured. Note that shock waves can be confined in the narrow region consisted of about two meshes,

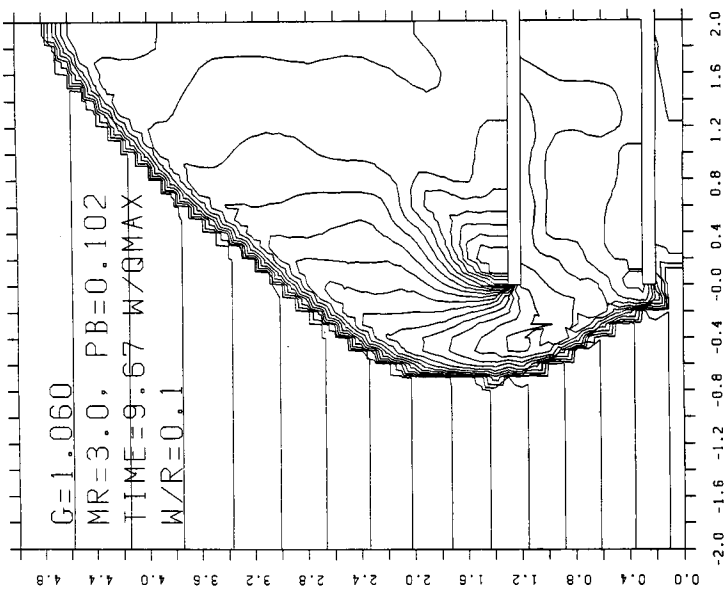

Figure 8. Pressure contours for stratified supersonic flow at $M_R = 3{\cdot}0$, inlet width/scale height = 0·954, $P_B = 0{\cdot}12$, 51 × 41 grid

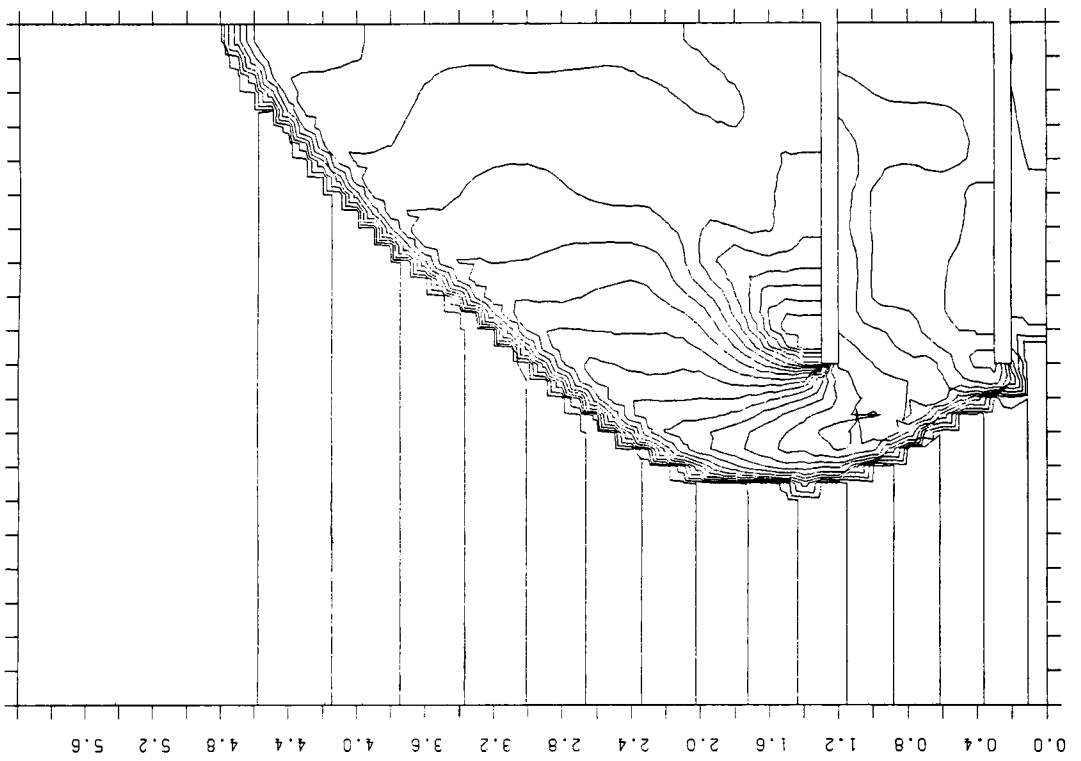

Figure 7. Pressure contours for stratified supersonic flow at $M_R = 3{\cdot}0$, inlet width/scale height = 0·954, $P_B = 0{\cdot}12$, 61 × 41 grid

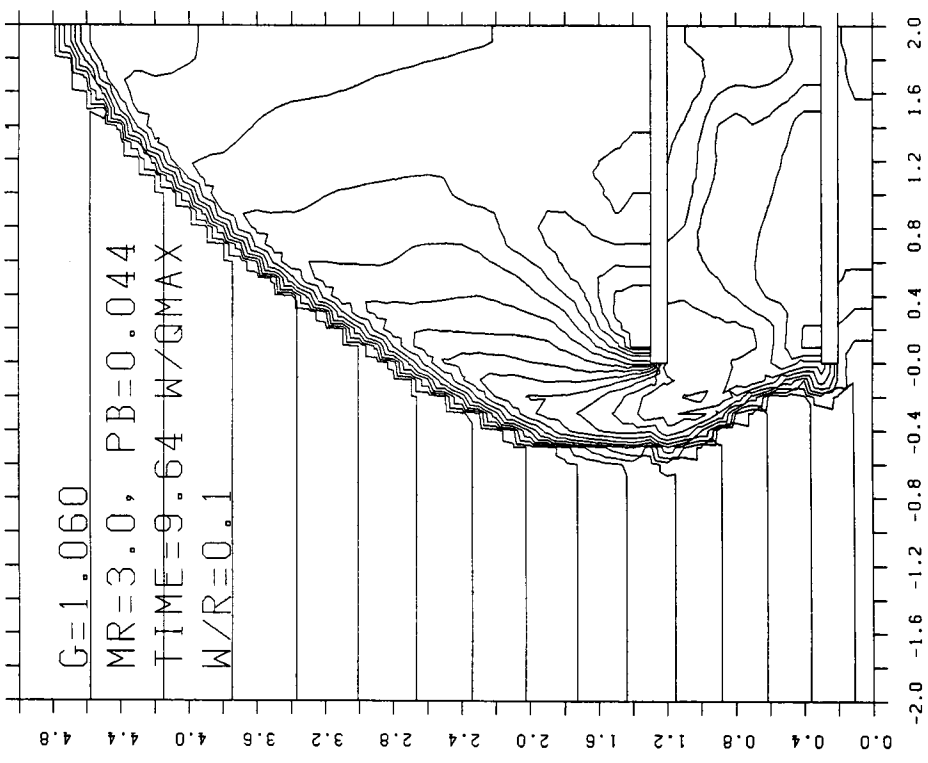

Figure 10. Pressure contours for stratified supersonic flow at $M_R = 3{\cdot}0$, inlet width/scale height $= 0{\cdot}954$, $P_B = 0{\cdot}044$

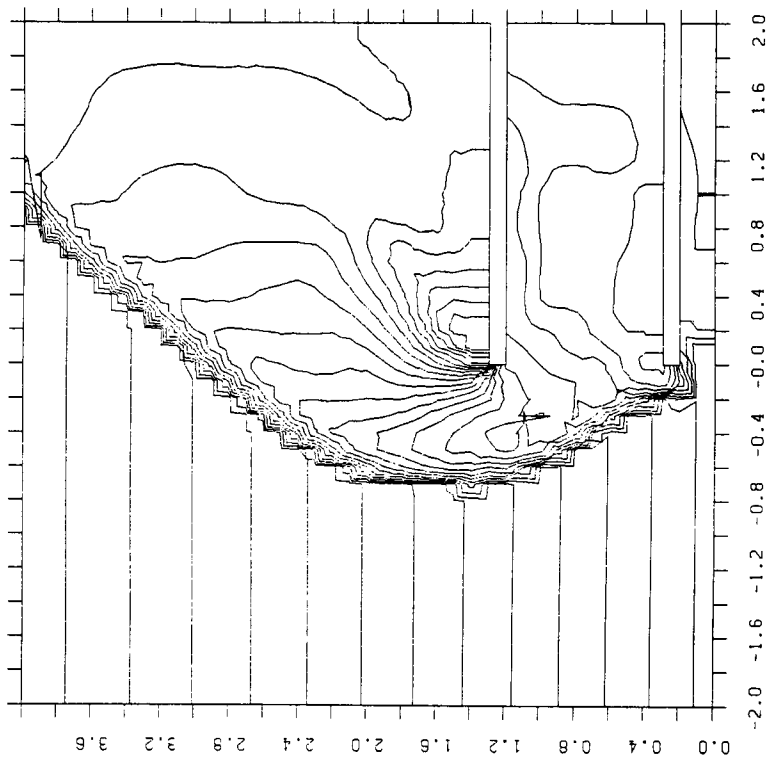

Figure 9. Pressure contours for stratified supersonic flow at $M_R = 3{\cdot}0$, inlet width/scale height $= 0{\cdot}954$, $P_B = 0{\cdot}12$, 41×41 grid

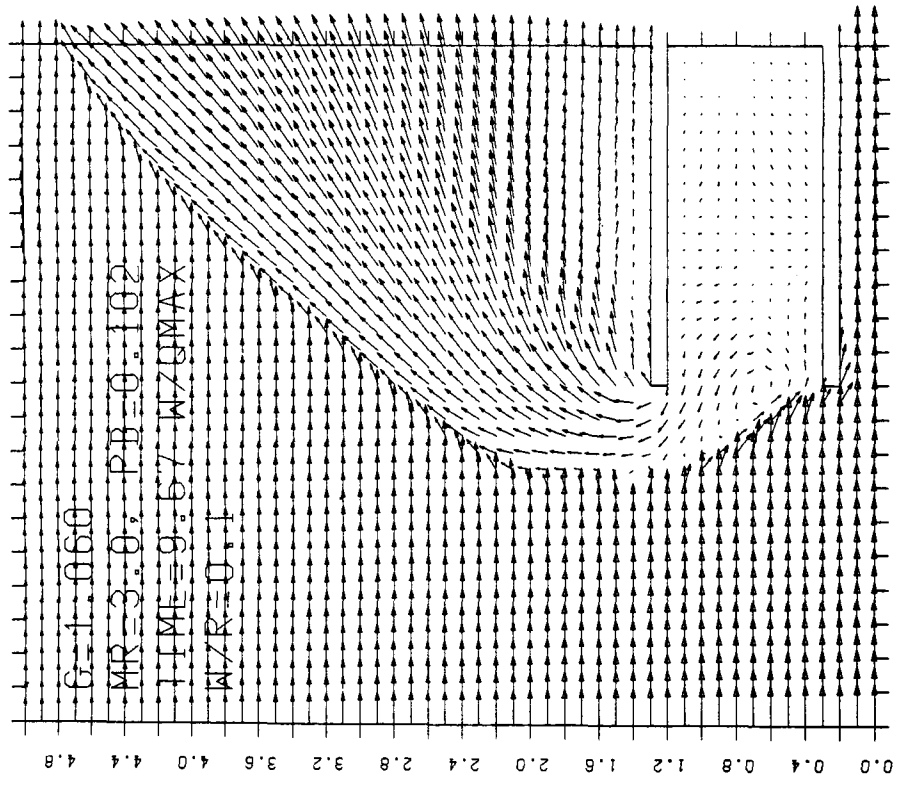

Figure 12. Velocity vector field for stratified supersonic flow at $M_R = 3{\cdot}0$, inlet width/scale height = 0·954, $P_B = 0{\cdot}12$

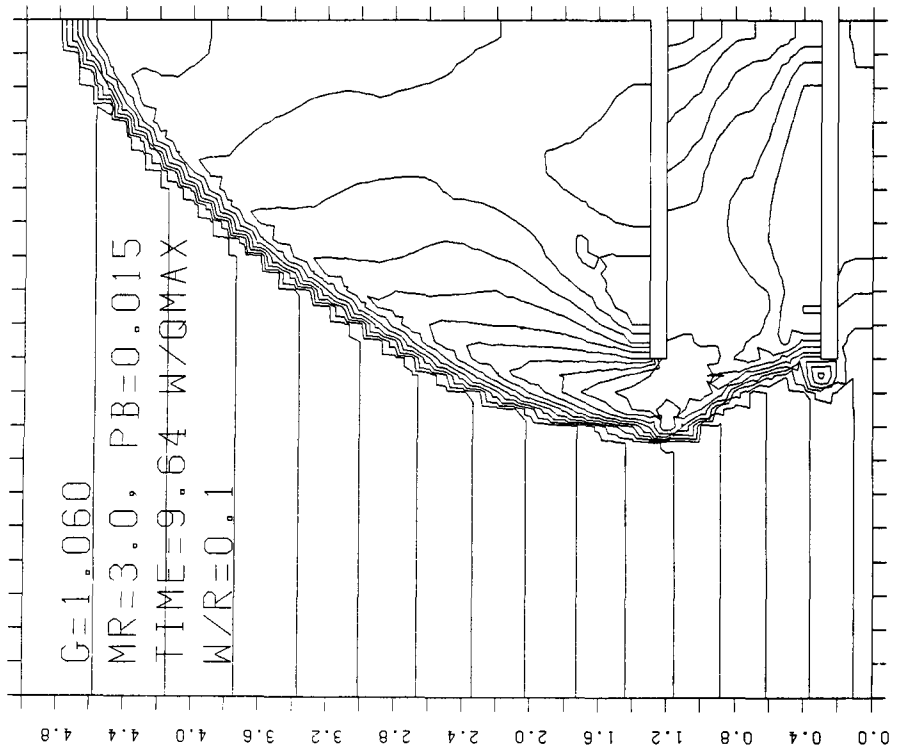

Figure 11. Pressure contours for stratified supersonic flow at $M_R = 3{\cdot}0$, inlet width/scale height = 0·954, $P_B = 0{\cdot}015$

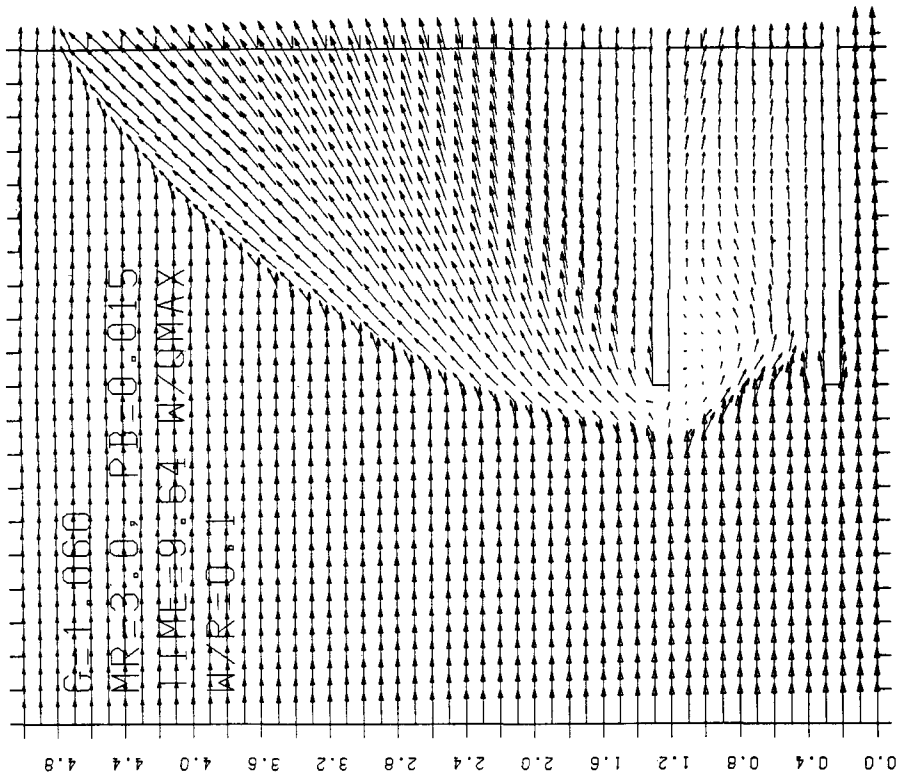

Figure 13. Velocity vector field for stratified supersonic flow at $M_R = 3{\cdot}0$, inlet width/scale height $= 0{\cdot}954$, $P_B = 0{\cdot}044$

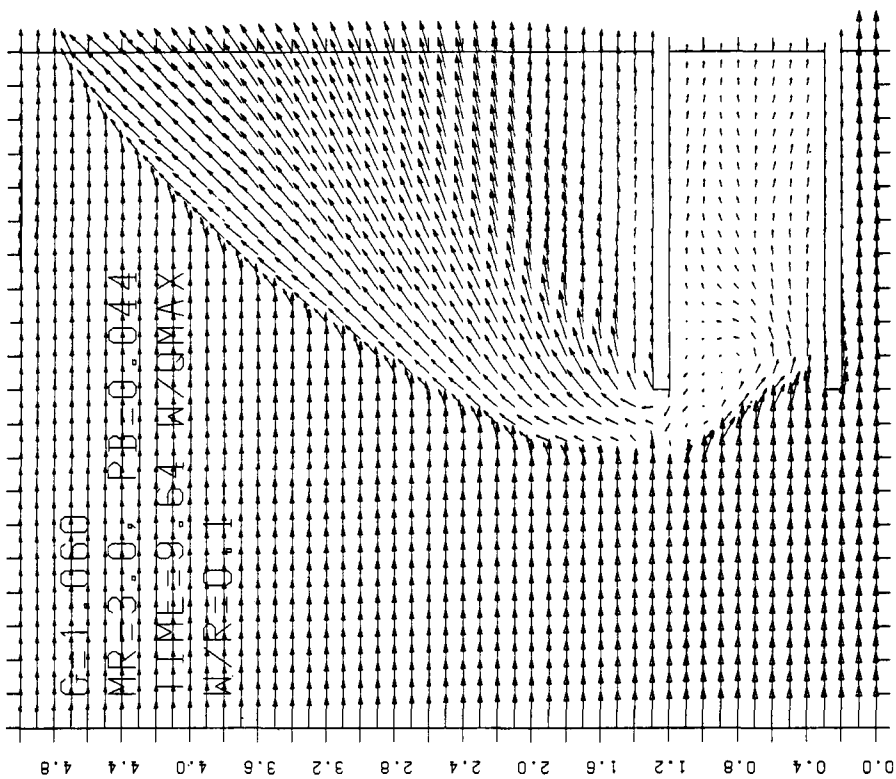

Figure 14. Velocity vector field for stratified supersonic flow at $M_R = 3{\cdot}0$, inlet width/scale height $= 0{\cdot}954$, $P_B = 0{\cdot}015$

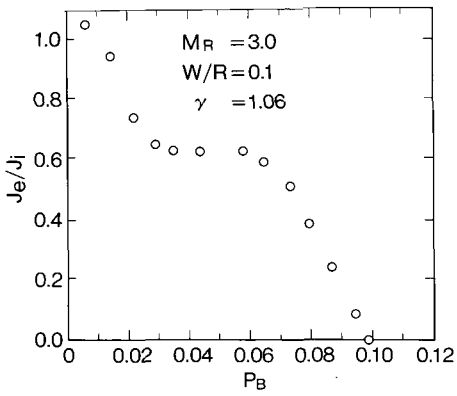

Figure 15. Extracted mass flow rate plotted against back pressure

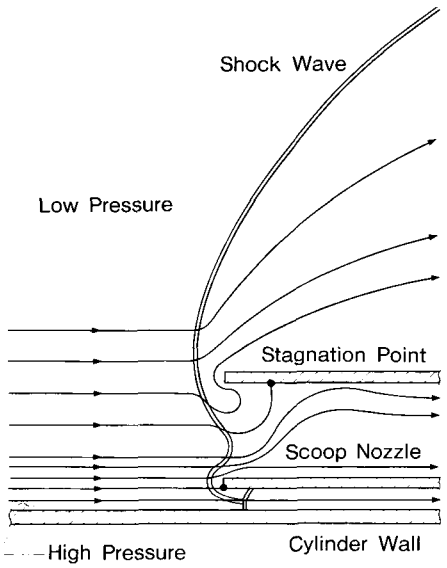

Figure 16. Schematic illustration of flow pattern

demonstrating an advantage of the PLM scheme over the 'shock capturing' schemes which significantly smear shock waves.

Of particular interest is the formation of an oblique shock wave in front of the almost whole portion of the inlet entrance. The incoming streamlines deflect towards the higher pressure side after passing through the oblique shock wave and then bend down to the lower pressure side, creating a centrifugal force to balance the strong pressure gradient in the radial direction, originating from the radial pressure gradient in the free stream, where the force balance in the r-direction is given in terms of the azimuthal velocity, v, and the radius of the rotating cylinder, R:

$$(\text{grad}\, p)\cdot \mathbf{e}_r = \frac{\rho v^2}{R}. \tag{70}$$

The azimuthal velocity decreases remarkably after passing through the shock wave, whereas the radial pressure gradient remains without a significant change. Thus, the radius of the curvature of the streamline should become much less than R to guarantee the force balance.

With decreasing the back pressure, the oblique shock wave ahead of the inlet nozzle moves closer to the entrance and a part of the shock wave is swallowed into the nozzle, thereby creating a small bow shock wave in front of the blunt leading edge locating on the high pressure side (see Figure 11). A part of the oblique shock wave is also swallowed into the gap between the nozzle wall and the wall of the rotating cylinder, at which the shock wave reflects. Note that the streamtube separating the extracted and unextracted flows expands along the inlet nozzle length. Thus, the flow field inside the nozzle resembles that in a duct of variable cross-sectional area. It is remarkable that one of the stagnation points is located inside the inlet nozzle. Regardless of the value of the back pressure, there appears a reverse flow in the vicinity of the leading edge on the low pressure side. The flow spills over it and in so doing undergoes a Prandtl–Meyer expansion followed by a recompression downstream of the external wall of the inlet nozzle. The extracted mass flow rate into the nozzle is much less than the flow rate estimated by assuming a parallel incoming stream even for low back pressures, as expected from the numerically generated flow field. The calculated mass flow normalized to that of the incoming parallel stream is plotted in Figure 15 as a function of the back pressure. Based on the flow field generated from the numerical results a qualitative flow model as shown in Figure 16 can be constructed for a rotating supersonic flow impinging upon a stationary inlet nozzle.

Computations were performed at Tokyo Institute of Technology, the program being developed and run on the computer HITAC-M280H of the computing centre which can handle about 13 million instructions per second. The CPU time required for each calculation was about five minutes.

ACKNOWLEDGEMENT

The present author thanks Dr. A. Melten of URNIT, West Germany, for providing his Fortran computer program for contour plots which has been conveniently used in the present work.

REFERENCES

1. H. Mikami, 'Rotating supersonic flow about scoop inlet using an unsteady implicit technique', *Bull. Res. Lab. Nucl. Reactors, Tokyo Institute of Technology*, **8**, 29–52 (1983).
2. B. Van Leer, 'Towards the ultimate conservative difference scheme. V. A second-order sequel to Godunov's method', *J. Comp. Physics*, **32**, 101–136 (1979).
3. G. A. Sod, 'A hybrid random choice method with application to internal combustion engines', in H. Cabanes, M. Holt and V. Rusanov (eds), *Proceedings of the Sixth International Conference on Numerical Methods in Fluid Dynamics*, Tbilisi, USSR, June 1978, pp. 492–501.
4. P. Colella and P. R. Woodward, 'The piecewise parabolic method (PMM) for gas-dynamical simulations', *J. Comp. Physics*, **54**, 174–201 (1984).
5. T. Saito and I. I. Glass, 'Application of random-choice method to problems in shock and detonation-wave dynamics', *UTIAS Report No. 240*, Institute for Aerospace Studies, University of Toronto, October 1979.
6. P. J. Roache, *Computational Fluid Dynamics*, Hermosa publishers, Albuquerque, New Mexico, U.S.A., 1972, pp. 282–283.